Ammonia-induced Seed Layer Transformations in A Hydrothermal Growth Process of Zinc Oxide Nanowires

Quanli Liu[1], Takao Yasui[1, 2]*, Kazuki Nagashima[3]*, Takeshi Yanagida[3, 4, 5], Mitsuo Hara[6], Masafumi Horiuchi[1], Zetao Zhu[1], Hiromi Takahashi[1], Taisuke Shimada[1], Akihide Arima[1] and Yoshinobu Baba[1, 7]*

[1] Department of Biomolecular Engineering, Graduate School of Engineering, Nagoya University, Furo-cho, Chikusa-ku, Nagoya 464-8603, Japan

[2] Japan Science and Technology Agency (JST), Precursory Research for Embryonic Science and Technology (PRESTO), 4-1-8 Honcho, Kawaguchi, Saitama 332-0012, Japan

[3] Department of Applied Chemistry, School of Engineering, The University of Tokyo, 7-3-1 Hongo, Bunkyo-ku, Tokyo 113-8656, Japan

[4] Institute of Materials Chemistry and Engineering, Kyushu University, 6-1 Kasuga-Koen, Kasuga, Fukuoka 816-8580, Japan

[5] Institute of Scientific and Industrial Research, Osaka University, 8-1 Mihogaoka-cho, Ibaraki, Osaka 567-0047, Japan

[6] Department of Molecular and Macromolecular Chemistry, Graduate School of Engineering, Nagoya University, Furo-cho, Chikusa-ku, Nagoya 464-8603, Japan

[7] Health Research Institute, National Institute of Advanced Industrial Science and Technology (AIST), Takamatsu 761-0395, Japan

*E-mail: yasui@chembio.nagoya-u.ac.jp.

*E-mail: kazu-n@g.ecc.u-tokyo.ac.jp.

*E-mail: babaymtt@chembio.nagoya-u.ac.jp.

Abstract

Ammonia is a well-known additive to promote the crystal growth in hydrothermal synthesis of ZnO nanowires. Although the effect of ammonia on the nanowire growth has been intensively investigated, an influence for the seed layer, which governs the initial nanowire growth, is rarely discussed. Here we demonstrate that ammonia strongly affects the seed layer as well as the following nanowire growth. When increasing the ammonia concentration, the nanowire density first increases and then decreases while the nanowire growth rate keeps increasing. Experimental results and thermodynamic calculations as to the initial growth process reveal that the transformation of seed layer induced by ammonia prior to the nucleation critically determines the nanowire density and thus also influences the following nanowire growth. Present results highlight the critical importance to discuss the variation of seed layer in ammonia-contained hydrothermal synthesis and suggest a novel seed engineering approach for tailoring the ZnO nanowire growth.

1. Introduction

Single crystalline zinc oxide (ZnO) nanowires have recently been extending their application fields from previous optics and electronics to newly emerging nano-bio analysis due to the various fascinating features including wide direct bandgap,[1, 2] large exciton binding energy,[1-3] piezoelectricity,[4, 5] Lewis acidity,[6, 7] high isoelectric point[8] and biocompatibility.[9, 10] Thanks to such variety of features, unique devices including light emitting diode (LED), nanogenerator, bio/chemical sensors and biomedical analysis devices have been demonstrated so far using ZnO nanowires.[11-15] A hydrothermal synthesis is among the most broadly utilized technique for fabricating the ZnO nanowires.[16-18] This is because the hydrothermal process is conducted at low temperature less than 100 ºC and the diameter/position of nanowires are designable via seed crystals. These allow us to integrate the ZnO nanowires with various materials and devices on a substrate.[19, 20] Fundamentally, the anisotropic crystal growth of ZnO nanowires originates from a preferential nucleation on ZnO (0001) plane, which is dominated by zinc hydroxide complexes ($Zn(OH)_n$) precursor.[21-23] Ammonia is a well-known additive to promote the ZnO nanowire growth.[24-28] Such ammonia effect has been interpreted in terms of the variations of ionic species in aqueous solution and their electrostatic interactions with ZnO crystal planes.[22, 29] Recent study by Sakai *et al.* further revealed that the increase of growth rate is mainly due to the change of rate limiting process from the precursor diffusion process to the ligand exchange process, which is caused by the decreased concentration of $Zn(OH)_n$.[21] On the other hand, the ammonia causes a dissociation of ZnO during the nanowire growth. The sharp and

uniformly-shaped nanowire tips were formed as a result of ammonia-induced face-selective etching on ZnO $\{10\bar{1}1\}$ planes.[30, 31] By using this etching effect, Zhao *et al.* demonstrated the synthesis of monodispersedly sized ZnO nanowires from randomly sized seeds.[31] The role of ammonia on the nanowire growth has been intensively investigated as described above, however, an influence for the seeds, which govern the nanowire growth, is rarely discussed. Clarifying how ammonia influences the seeds is of crucial importance to comprehensively understand and tailor the ammonia-induced ZnO nanowire growth. Thus, in this study, we investigate the ammonia effect on seeds in hydrothermal synthesis of ZnO nanowires. We found that ammonia transforms the seed layer prior to nucleation and strongly affects the following nanowire growth.

2. Experimental section

ZnO nanowire growth was conducted by a hydrothermal synthesis. First, 20 mm × 10 mm silicon substrates (N-type) were cleaned in a mixture of 98 % sulfuric acid and 35 % hydrogen peroxide with volume ratio of 3:1 at 180 ºC for 2 h. After cooling down to room temperature, the substrates were taken out from the cleaning solution, washed by ultrapure water and dried by blowing nitrogen gas. The ZnO seed layer was then deposited on the substrate by radio frequency (RF) sputtering with RF power of 50 W under ambient pressure of 1 Pa with Ar:O_2 ratio of 5:1 at room temperature. The deposition rate of ZnO seed layer was 10 nm/ min. The thickness of ZnO seed layer was controlled to be 75 nm, where the highest areal density of uniformly shaped nanowires is available (see Supporting Information figure S1). The nanowire growth

solution was prepared by mixing zinc nitrate hexahydrate ($Zn(NO_3)_2 \cdot 6H_2O$, 40 mM), hexamethylenetetramine (HMTA, 40 mM) and ammonia solution (25 wt.%) with varying the concentration in a range of 0-1000 mM at room temperature. The seed layer coated substrates were immersed into Teflon cups filled with 50 ml of growth solution in a manner of upside down. Then the Teflon cups were put into the oven set at 95 ºC. The growth time was varied in between 10-180 min. After the growth, the samples were washed by ultrapure water and acetone, then dried at 80 °C for 10 min. The morphologies of ZnO seed layer and ZnO nanowires were evaluated by a scanning electron microscope (SEM; Zeiss Supra 40 VP). The ZnO nanostructures constructed at early stage were characterized by a grazing-incidence x-ray diffraction (GI-XRD; Rigaku FR-E). For GI-XRD, a radiation source of Cu Kα (λ = 0.154 nm) was used and the incident angle of the beam to the sample surface was adjusted at about 0.18−0.22º.

3. Results and discussion

Figure 1A shows the cross-sectional SEM images of ZnO nanowires grown for 3 h with varying ammonia concentration (C_{NH3}) of 0-1000 mM. When increasing C_{NH3}, the nanowire growth rate increases. The observed trend is consistent with many previous studies, which can be interpreted in terms of the variations of ionic species in aqueous solution, their electrostatic interactions with ZnO crystal planes and the rapid ligand exchange process between different zinc complexes.[21-28] On the other hand, the areal number density of nanowire (hereafter nanowire density) and the diameter show unique trends as explained in the followings. Figure 1B shows the quantitative C_{NH3}

dependences on the nanowire density and the diameter. We found that the nanowire density tends to first increase and then decrease with increasing C_{NH3}, and the diameter inversely correlates with the nanowire density. These trends cannot be explained by the ammonia-induced crystal growth promotion. Although the diameter is affected by various factors, the observed correlation indicates that the diameter is predominantly determined by a material competition effect between adjacent nanowires.[32] Thus, these results show that ammonia affects not only the nanowire growth rate but also the nanowire density and the diameter.

We found that the seed layer located at the bottom of nanowires tends to be thinner with increasing C_{NH3}, as shown in figure 1A and 1C. This result indicates the significant effect of ammonia on the seed layer and therefore strongly recommends to observe the seed layer at the initial growth process, although it has been rarely discussed previously. Figure 2A shows SEM images of the seed layer observed after 10-30 min of growth process with various C_{NH3}. At relatively low C_{NH3} range of 0-600 mM, the nanowire growth immediately occurs within 20 min. In this condition, the nanowire density tends to increase with increasing C_{NH3}. On the other hand, at relatively high C_{NH3} range of 800-1000 mM, the seed layer seems to be removed from the substrate and none of nanowire growth can be seen. We found that the seed layer is removed within first 10 min and the nanoparticles tend to form in the following 20 min. The variations of nanowire/nanoparticle density observed at the initial growth process is consistent with that of the nanowire density in figure 1B, suggesting that the nanowire density is determined by the morphology of seed layer formed at the initial growth process. Thus

the result in figure 2A clearly evidences that ammonia strongly affects the seed layer at initial growth process as well as the following nanowire growth.

Here we consider how ammonia affects the seed layer at the initial growth process. First, we discuss the increasing trend of nanowire density with increasing C_{NH3} at relatively low concentration range. Since the seed layer fully covers the substrate in this C_{NH3} range, the variation of nanowire density should be determined by the nucleation phenomena on the seed layer. As seen in figure 1A, a nanowire is grown from several seed crystals at C_{NH3} 0 mM while it tends to grow from individual seed crystal by increasing C_{NH3}. This trend can be interpreted in terms of the suppression of nuclei merge via ammonia induced sharp tip formation as demonstrated by our previous study.[31] When using the densely deposited seed crystals, the adjacent nuclei spontaneously merge during the nanowire growth and this leads to the decrease of nanowire density. In the previous study, we found that the sharp tip seeds formed by ammonia-based etching provide the spatially separated nucleation sites and suppress the merge of nuclei. Since the sharp tip formation on seeds is promoted by increasing C_{NH3}, this might lead the increase of nanowire density at relatively low concentration range.

Next, we discuss the decreasing trend of nanowire density with increasing C_{NH3} at relatively high concentration range. According to the results in figure 1C and 2A, we assume that the seed layer is dissociated prior to the nucleation and the number of remaining seeds might determine the nanowire density. In fact, the pH becomes over 11 by introducing 800 mM ammonia (see Supporting Information figure S2), which is

high enough for dissociating ZnO.[31, 33] Figure 2B shows the Zn mapping of seed layers characterized by energy dispersive spectroscopy (EDS). The images were taken from the initial seed layer and after 10-30 min of growth process with various C_{NH3} (the all data is shown in Supporting Information figure S3). We found that the seeds are inhomogeneously distributed at C_{NH3} 800 mM and only the sparsely distributed nanoparticles are seen at C_{NH3} 1000 mM. More specifically, the relative Zn intensity normalized by the initial ZnO seed layer decreases by 88-90 % after 10 min of growth process at C_{NH3} 800-1000 mM (figure 2C). These results clearly evidence that the seed layer is dissociated during initial growth process at relatively high C_{NH3} range.

We also found in figure 2B that the seed density increases by extending the growth time to 30 min, which is consistent with the result in figure 2A and confirmed as the variation of Zn intensity in figure 2C. In order to specify the variation of seed crystals observed above, we performed GI-XRD measurement with varying the growth time in figure 2D. In this experiment, the samples of C_{NH3} 800 mM were evaluated. There found two trends as to the variation of seed crystals. First, when increasing the growth time, the ZnO (002) peak intensity initially decreases at 10 min and then increases at 30 min as consistent with results in figure 2A-2C. This indicates that the seed crystals are reconstructed after the dissociation. Second, although only the ZnO (002) peak is observable in the initial seed layer, (100) peak and (101) peak also tend to appear with increasing the growth time, showing that the variously oriented seed crystals are reconstructed after the dissociation. Such reconstructed seed crystals led to the variety of orientation in the nanowires grown at high C_{NH3} condition (see figure 1A). Note that

the seed density at 30 min of growth time is very similar to that observed in figure 1A. Thus, these results highlight that the nanowire density at high C_{NH3} condition is strongly governed via dissociation and reconstruction of seed crystals.

To gain the in-depth insight for the experimental results observed above, we performed the thermodynamic calculations at given growth conditions. In this calculation, the solubility of ZnO, i.e. the saturated Zn concentration, was estimated by involving all of related zinc ions existing in the growth solution. The details of calculation are seen in Supporting Information S4. The pH value and the temperature of growth solution were measured at each growth time and utilized for estimating the solubility (see Supporting Information figure S1). Figure 3A and 3B respectively show the pH dependent solubility of ZnO with various C_{NH3} at 25 ºC and 60 ºC, where 60 ºC is associated with the growth time of 10-20 min. Note that the dotted lines and the filled circles in the figures represent the Zn concentration used for the nanowire growth and the solubility of ZnO at the measured pH condition, respectively. At relatively low C_{NH3} range (i.e. 400-600 mM), the growth solution is almost saturated at 25 ºC and supersaturated at 60 ºC. This result shows the good consistency with the results of figure 2A, of which the nanowire growth immediately occurs after 10 min of growth time at this condition. Contrary, at relatively high C_{NH3} range (i.e. 800-1000 mM), the growth solution is not saturated and afford to dissociate ZnO at 25 ºC while it becomes supersaturated by increasing temperature up to 60 ºC. Such temperature dependence observed at higher C_{NH3} range is consistent with previous study, where $Zn(NH_3)_4^{2+}$ ions dominate the solubility of ZnO in ammonia-added aqueous solution.[22] In fact, our

calculations revealed that the solubility of ZnO in our experimental conditions is governed by the concentration of $Zn(NH_3)_4^{2+}$ ions (see Supporting Information figure S5). Thus the dynamic change of saturation degree induced by temperature variation reasonably explain why the seed layer is dissociated at first and then reconstructed during the initial growth process.

4. Conclusions

In conclusion, we investigated the effect of ammonia on the seed layer in hydrothermal synthesis of ZnO nanowires, which had been rarely discussed previously. The nanowire growth rate increased accompanying with the increase of C_{NH3} as consistent with many previous studies. On the contrary, the nanowire density and the diameter exhibited the unique tendencies, of which the nanowire density first increased then decreased with increasing C_{NH3} and the diameter inversely correlated with the nanowire density. The detailed experimental analysis revealed that the transformation of seed layer occurs prior to the nucleation and critically determines the features of fabricated nanowires including the nanowire density and the diameter. There found that the nanowire density is governed by two dominant transformations of the seed layer, i.e. the formation of sharp tips on the seed increases the nanowire density by suppressing the merge of adjacent nuclei at relatively low C_{NH3} range, and the dissociation of seed layer decreases the nanowire density at relatively high C_{NH3} range. We also found that at relatively high C_{NH3} range the seed crystals were reconstructed after the dissociation. Thermodynamic calculation revealed that the variation of

saturation degree at initial growth process is responsible for the reconstruction of seed crystals. Our results highlight that observing the variation of seed layer at initial growth process is of critical importance to understand the comprehensive growth mechanism in ammonia-contained hydrothermal ZnO nanowire synthesis and also suggest a novel seed engineering approach for tailoring the ZnO nanowire growth.

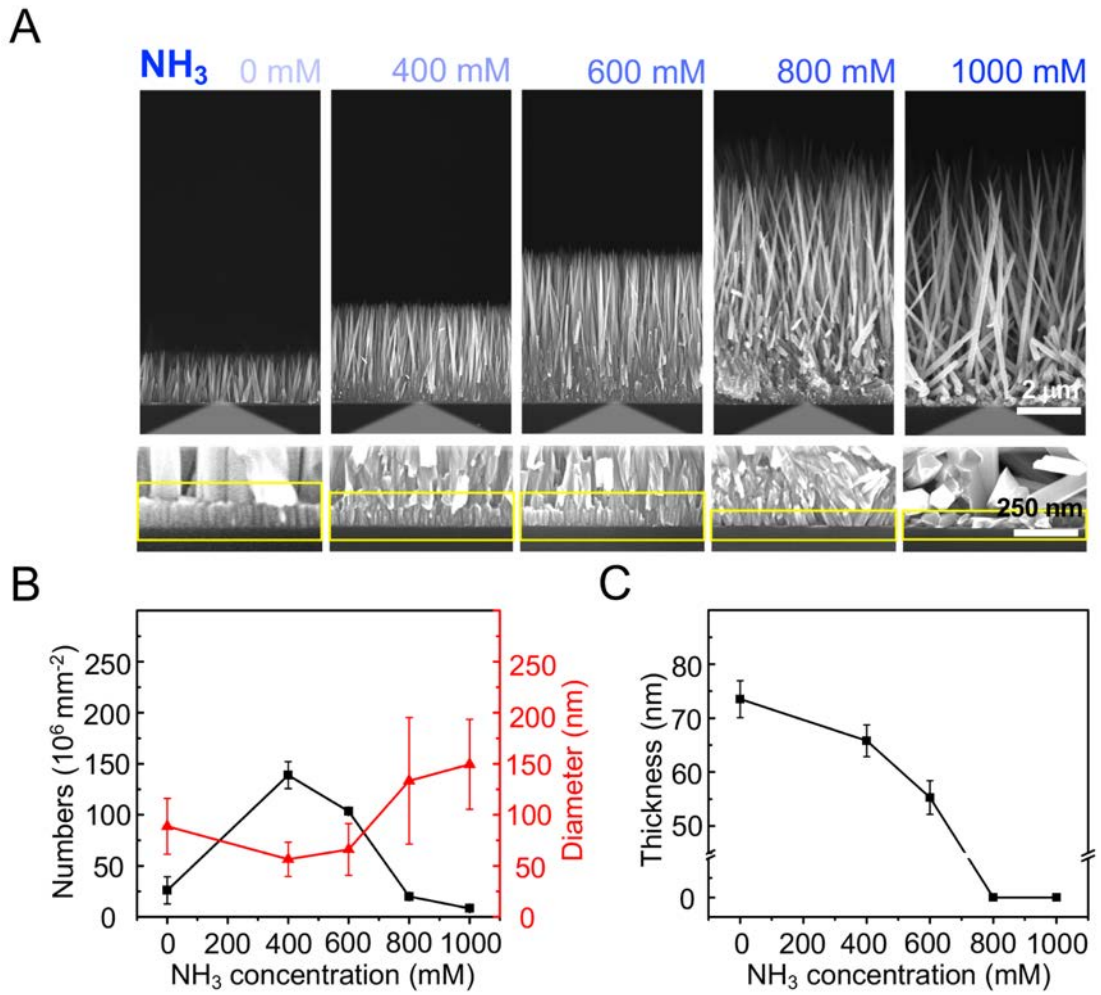

Figure 1. SEM images and statistical analysis of nanowires grown in various concentrations of ammonia after growth time for 3 h. **A.** Nanostructure morphology variation from horizontal direction with increase of ammonia concentrations. Yellow squares are enlarged views of nanowire roots. Images in the same row use the same scale bars. **B**. Nanowire areal density and diameter in various concentrations of ammonia. Error bars show the standard deviation for a series of measurements (for nanowires number: N = 10, for diameter: N= 100). **C**. Thickness of ZnO seed layer in various concentrations of ammonia. Error bars show the standard deviation for a series of measurements (N = 3).

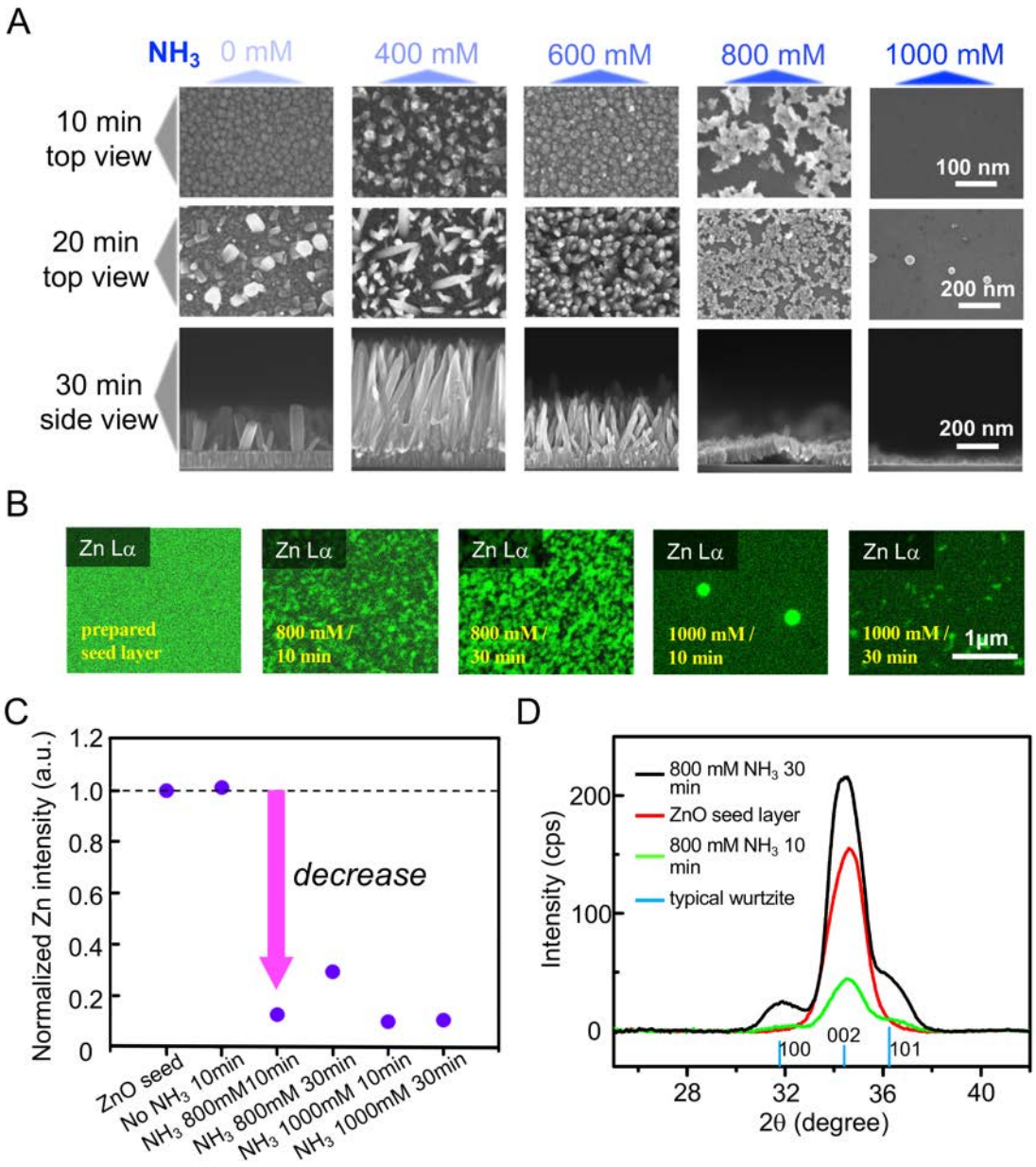

Figure 2. Characteristics of ZnO seed layers. **A**. SEM images of synthesis products at the initial 10, 20 and 30 min. Product morphologies varied with increase of ammonia concentrations. Images in the same row have the same scale bar as given in the last image of the row. **B**. EDS mapping analysis of seed layer transformation after immersing into growth solution with 800 and 1000 mM ammonia for 10 and 30 min respectively. **C**. Normalized Zn intensity of the substrate during the initial 30 min of

the hydrothermal process. Images have the same scale bar as given in the last image of the row. **D**. GI-XRD profiles of prepared ZnO seed layer and prepared ZnO seed layer after immersing into growth solution with 800 mM ammonia addition for 10 and 30 min. Vertical light blue lines indicate typical wurtzite (JCPDS NO. 36- 1451) peak positions.

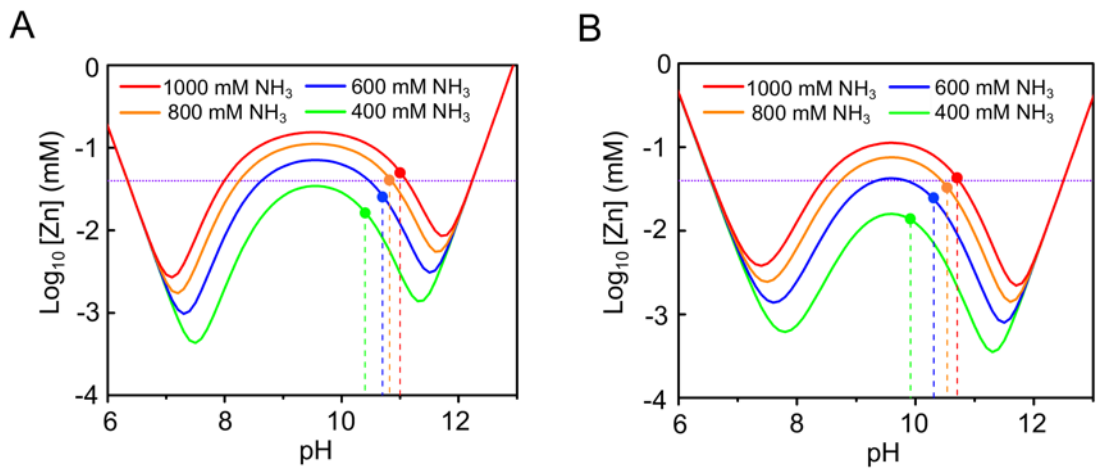

Figure 3. pH value dependent theoretical solubility of Zn(II) in aqueous solutions with varied concentrations of ammonia. **A.** pH value dependent theoretical solubility of Zn(II) in aqueous solutions with varied concentrations of ammonia at 25 ºC. **B.** pH value dependent theoretical solubility of Zn(II) in aqueous solutions with varied concentrations of ammonia at 60 ºC. Intersection points of solid curve and dash line in the same color represent theoretical solubility of Zn(II) at corresponding measured pH values. Horizontal dotted line represents Zn(II) concentration in prepared aqueous solution, which equals to zinc nitrate hexahydrate concentration, 40 mM.

Acknowledgements

This research was supported by PRESTO (JPMJPR151B, JPMJPR19H9), Japan Science and Technology Agency (JST), the “Development of Diagnostic Technology for Detection of miRNA in Body Fluids” grant from the Japan Agency for Medical Research and Development and New Energy and Industrial Technology Development Organization, the JSPS Grant-in-Aid for Young Scientists (A) 17H04803, the JSPS

Grant-in-Aid for Scientific Research (A) 16H02091, the JSPS Grant-in-Aid for Scientific Research (S) 18H05243, a research grant from the Murata Science Foundation, Advanced Technology Institute Research Grants 2019, the Foundation of Public Interest of Tatematsu, the Nitto Foundation, and the Nanotechnology Platform Program (Molecule and Material Synthesis) of the Ministry of Education, Culture, Sports, Science and Technology (MEXT). We thank Dr. Daisuke Onoshima and Dr. Hiroshi Yukawa for their valuable discussions.

Supporting Information Available:

Figure S1 SEM images, diameter and areal density of ZnO nanowires grown with various seed layer thickness. The data was taken with growth time for 3 h and without NH_3.

Figure S2 pH value and temperature of growth solution over time.

Figure S3 EDS mapping analysis of seed layer on silicon substrate after immersing into growth solution with varied ammonia concentration for 10 and 30 min, respectively.

Figure S4 Thermodynamic calculation of Zn(II) solubility in aqueous solutions.

Figure S5 Speciation of dissolved Zn(II) versus pH and temperature in growth solution.

References

[1]Xu, S.; Wang, Z. L. One-dimensional ZnO nanostructures: Solution growth and functional properties. *Nano Res.* **2011**, *4*, 1013-1098.

[2]Özgür, Ü.; Alivov, Y. I.; Liu, C.; Teke, A.; Reshchikov, M. A.; Doğan, S.; Avrutin, V.; Cho, S. J.; Morkoç, H. A comprehensive review of ZnO materials and devices. *J. Appl. Phys.* **2005**, *98*, 041301.

[3]Thomas, D. G. The exciton spectrum of zinc oxide. *J. Phys. Chem. Solids* **1960**, *15*, 86-96.

[4]Wang, Z. L.; Song, H. Piezoelectric nanogenerators based on zinc oxide nanowire arrays. *Science* **2006**, *312*, 242-246.

[5]Groo, L.; Inman, D. J.; Sodano, H. A. In situ damage detection for fiber‐reinforced composites using integrated zinc oxide nanowires. *Adv. Funct. Mater.* **2018**, *28*, 1802846.

[6]Ballerini, G.; Ogle, K.; Barthés-Labrousse, M.-G. The acid–base properties of the surface of native zinc oxide layers: An XPS study of adsorption of 1,2-diaminoethane. *Appl. Surf. Sci.* **2007**, *253*, 6860-6867.

[7]Perez-Lopez, Q. W.; Farias, A. C.; Marcilio, N. R.; Bueno, J. M. C. The catalytic behavior of zinc oxide prepared from various precursors and by different methods. *Mater. Res. Bull.* **2005**, *40*, 2089-2099.

[8]Cao, L.; Kiely, J.; Piano, M.; Luxton, R. Facile and inexpensive fabrication of zinc oxide based bio-surfaces for C-reactive protein detection. *Sci. Rep.* **2018**, *8*, 12687.

[9] Dagdeviren, C.; Hwang, S.-W.; Su, Y.; Kim, S.; Cheng, H.; Gur, O.; Haney, R.; Omenetto, F. G.; Huang, Y.; Rogers, J. A. Transient, Biocompatible electronics and energy harvesters based on ZnO. *Small* **2013**, *9*, 3398-3404.

[10] Bhang, S. H.; Jang, W.; Han, J.; Yoon, J.-K.; La, W.-G.; Lee, E.; Kim, Y. S.; Shin, J.-Y.; Lee,T.-J.; Baik, H. K.; Kim, B.-S. Zinc oxide nanorod‐based piezoelectric dermal patch for wound healing. *Adv. Funct. Mater.* **2017**, *27*, 1603497.

[11] Bao, J.; Zimmler, M. A.; Capasso, F.; Wang, X.; Ren, Z. F. Broadband ZnO single-nanowire light-emitting diode. *Nano Lett.* **2006**, *6*, 1719-1722.

[12] Wang, X.; Song, J.; Liu, J.; Wang, Z. L. Direct-current nanogenerator driven by ultrasonic waves. *Science* **2007**, *316*, 102-105.

[13] Haarindraprasad, R.; Hashim, U.; Gopinath, S. C. B.; Perumal, V.; Liu, W.-W.; Balakrishnan, S. R. Fabrication of interdigitated high-performance zinc oxide nanowire modified electrodes for glucose sensing. *Anal. Chim. Acta* **2016**, *925*, 70-81.

[14] Xu, X.; Yan, M.; Tian, X.; Yang, C.; Shi, M.; Wei, Q.; Xu, L.; Mai, L. In situ investigation of Li and Na ion transport with single nanowire electrochemical devices. *Nano Lett.* **2015**, *15*, 3879-3884.

[15] Yasui, T.; Yanagida, T.; Ito, S.; Konakade, Y.; Takeshita, D.; Naganawa, K.; Nagashima, K.; Shimada, T.; Kaji, N.; Nakamura, Y.; Thiodorus, I. A.; He, Y.; Rahong, S.; Kanai, M.; Yukawa, H.; Ochiya, T.; Kawai, T.; Baba, Y. Unveiling

massive numbers of cancer-related urinary-microRNA candidates via nanowires. *Sci. Adv.* **2017**, *3*, e1701133.

[16] Cheng, J. J.; Nicaise, S. M.; Berggren, K. K.; Gradečak, S. Dimensional tailoring of hydrothermally grown zinc oxide nanowire arrays. *Nano Lett.* **2016**, *16*, 753-759.

[17] Cho, J.; Salleh, N.; Blanco, C.; Yang, S.; Lee, C.; Kim, Y.; Kim, J.; Liu, J. Novel synthetic methodology for controlling the orientation of zinc oxide nanowires grown on silicon oxide substrates. *Nanoscale* **2014**, *6*, 3861-3867.

[18] Qiu, J.; Li, X.; He, W.; Park, S.-J.; Kim, H.-K.; Hwang, Y.-H.; Lee, J.-H.; Kim, Y.-D. The growth mechanism and optical properties of ultralong ZnO nanorod arrays with a high aspect ratio by a preheating hydrothermal method. *Nanotechnology* **2009**, *20*, 155603.

[19] Ou, C.; Sanchez-Jimenez, P.; Datta, A.; Boughey, F. L.; Whiter, R. A.; Sahonta, S. L.; Kar-Narayan, S. Template-assisted hydrothermal growth of aligned zinc oxide nanowires for piezoelectric energy harvesting applications. *ACS Appl. Mater. Inter.* **2016**, *8*, 13678-13683.

[20] Azzouz, I.; Habba, Y. G.; Capochichi-Gnambodoe, M.; Marty, F.; Vial, J.; Leprince-Wang, Y.; Bourouina, T. Zinc oxide nano-enabled microfluidic reactor for water purification and its applicability to volatile organic compounds. *Microsyst. Nanoeng.* **2018**, *4*, 17093.

[21] Sakai, D.; Nagashima, K.; Yoshida, H.; Kanai, M.; He, Y.; Zhang, G.; Zhao, X.; Takahashi, T.; Yasui, T.; Hosomi, T.; Uchida, Y.; Takeda, S.; Baba, Y.; Yanagida,

T. Substantial narrowing on the Width of “concentration Window” of hydrothermal ZnO nanowires via ammonia addition. *Sci. Rep.* **2019**, *9*, 14160.

[22] He, Y.; Yanagida, T.; Nagashima, K.; Zhuge, F.; Meng, G.; Xu, B.; Klamchuen, A.; Rahong, S.; Kanai, M.; Li, X.; Suzuki, M.; Kai, S.; Kawai, T. Crystal-plane dependence of critical concentration for nucleation on hydrothermal ZnO nanowires. *J. Phys. Chem. C* **2013**, *117*, 1197-1203.

[23] Cossuet, T.; Appert, E.; Thomassin, J.-L.; Consonni, V. Polarity-dependent growth rates of selective area grown ZnO nanorods by chemical bath deposition. *Langmuir* **2017**, *33*, 6269-6279.

[24] Syrrokostas, G.; Govatsi, K.; Yannopoulos, S. N. High-quality, reproducible ZnO nanowire arrays obtained by a multiparameter optimization of chemical bath deposition growth. *Cryst. Growth Des.* **2016**, *16*, 2140-2150.

[25] Richardson, J. J.; Lange, F. F. Controlling low temperature aqueous synthesis of ZnO. 2. A novel continuous circulation reactor. *Cryst. Growth Des.* **2009**, *9*, 2576-2581.

[26] Kwon, T. H.; Kim, K.; Park, S. H.; Annamalai, A.; Lee, M. J. Effect of seed particle size and ammonia concentration on the growth of ZnO nanowire arrays and their photoconversion efficiency. *Int. J. Nanotechnol.* **2013**, *10*, 681-691.

[27] Boubenia, S.; Dahiya, A. S.; Poulin-Vittrant, G.; Morini, F.; Nadaud, K.; Alquier, D. A facile hydrothermal approach for the density tunable growth of ZnO nanowires and their electrical characterizations. *Sci. Rep.* **2017**, *7*, 15187.

[28] Chen, L.-Y.; Yin, Y.-T.; Chen, C.-H.; Chiou, J.-W. Influence of polyethyleneimine and ammonium on the growth of ZnO nanowires by hydrothermal method. *J. Phys. Chem. C* **2011**, *115*, 20913-20919.

[29] Richardson, J. J.; Lange, F. F. Controlling low temperature aqueous synthesis of ZnO. 1. Thermodynamic analysis. *Cryst. Growth Des.* **2009**, *9*, 2570-2575.

[30] Wang, H. Q.; Li, G. H.; Jia, L. C.; Wang, G. Z.; Li, L. General in situ chemical etching synthesis of ZnO nanotips array. *Appl. Phys. Lett.* **2008**, *93*, 153110.

[31] Zhao, X.; Nagashima, K.; Zhang, G.; Hosomi, T.; Yoshida, H.; Akihiro, Y.; Kanai, M.; Mizukami, W.; Zhu, Z.; Takahashi, T.; Suzuki, M.; Samransuksamer, B.; Meng, G.; Yasui, T.; Aoki, Y.; Baba, Y.; Yanagida, T. Synthesis of monodispersedly sized ZnO nanowires from randomly sized seeds. *Nano Lett.* **2020**, *20*, 599-605.

[32] Lee, J. M.; No, Y.-S.; Kim, S.; Park, H.-G.; Park, W. I. Strong interactive growth behaviours in solution-phase synthesis of three-dimensional metal oxide nanostructures. *Nat. Commun.* **2015**, *6*, 6325.

[33] Zhou, J. Xu, N. S.; Wang, Z. L. Dissolving behavior and stability of ZnO wires in biofluids: A study on biodegradability and biocompatibility of ZnO nanostructures. *Adv. Mater.* **2006**, *18*, 2432-2435.

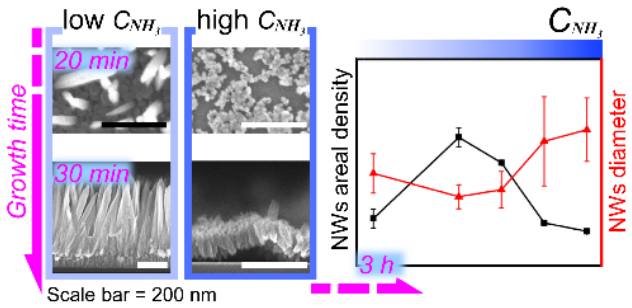

For Table of Contents Only